Paper:
Creasy, R., Mostert, B., Solemanifar, A., Nguyen, T., Virdis, B., Freguia, S. & Laycock, B. (2019). Biomimetic Peptide Nanowires Designed for Conductivity. *ACS Omega, 4*(1), 1748-1756.
http://dx.doi.org/10.1021/acsomega.8b02231

ACS OMEGA

Article

Cite This: ACS Omega 2019, 4, 1748−1756

http://pubs.acs.org/journal/acsodf

Biomimetic Peptide Nanowires Designed for Conductivity

Rhiannon C. G. Creasey,*[,†] A. Bernardus Mostert,[§] Armin Solemanifar,[†] Tuan A. H. Nguyen,[†,∥] Bernardino Virdis,[‡] Stefano Freguia,[‡] and Bronwyn Laycock*[,†]

[†]School of Chemical Engineering and [‡]Advanced Water Management Centre, The University of Queensland, St Lucia, QLD 4072, Australia

[§]Department of Chemistry, Swansea University, Singleton Park, Swansea, Wales SA2 8PP, U.K.

Supporting Information

ABSTRACT: The filamentous peptide-based nanowires produced by some dissimilatory metal-reducing bacteria, such as *Geobacter sulfurreducens*, display excellent natural conductivity. Their mechanism of conduction is assumed to be a combination of delocalized electrons through closely aligned aromatic amino acids and hopping/charge transfer. The proteins that form these microbial nanowires are structured from a coiled-coil, for which the design rules have been reported in the literature. Furthermore, at least one biomimetic system using related synthetic peptides has shown that the incorporation of aromatic residues can be used to enhance conductivity of peptide fibers. Herein, the de novo design of peptide sequences is used to enhance the conductivity of peptide gels, as inspired by microbial nanowires. A critical factor hampering investigations in both microbiology and materials development is inconsistent reporting of biomaterial conductivity measurements, with consistent methodologies needed for such investigations. We have reported a method herein to analyze non-Ohmic behavior using existing parameters, which is a statistically insightful approach for detecting small changes in biologically based samples. Aromatic residues were found to contribute to peptide gel conductivity, with the importance of the peptide confirmation and fibril assembly demonstrated both experimentally and computationally. This is a small step (in combination with parallel research under way by other researchers) toward developing effective peptide-based conducting nanowires, opening the door to the use of electronics in water and physiological environments for bioelectronic and bioenergy applications.

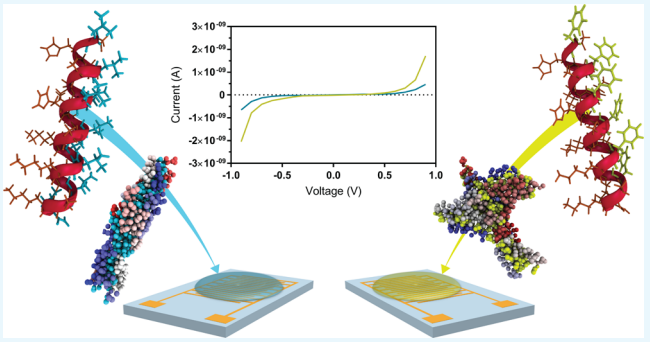

INTRODUCTION

The mechanism of conductivity in the microbial nanowires of *Geobacter sulfurreducens* has been controversially proposed to occur through electron delocalization in closely stacked aromatic amino acids.[1−3] Band conduction of this nature is a novel phenomenon in natural systems, with wide-reaching implications for protein functionality.[3,4] Furthermore, microbes play diverse roles in the biogeochemistry of anaerobic soils and sediments; understanding the manner of electron transport in such natural systems is integral to bioremediation and bioenergy strategies.[5−10] In addition, bioelectronics is an emerging discipline at the interface of biology and electronics, reacting to a strong demand for flexible, biocompatible, and naturally derived electronically active materials.[11,12] Peptide-based mimics of microbial nanowires appear to be ideal candidates for self-assembling bioelectronic materials.[13]

The de novo design and application of self-assembling peptides is an established strategy for bionanotechnology applications.[14,15] Peptides offer a suite of biological and chemical functionalities exploitable for the formation of supramolecular architectures, such as ordered nanofibers. Hence, this approach is appropriate for mimicking conducting bacterial nanowires. Given that it is known that the PilA proteins of *G. sulfurreducens* utilize a coiled-coil motif for nanowire formation,[16] the design rules for forming α helices and coiled-coil structures can be applied, driven by siting hydrophobic amino acid side chains in the assembled fibril core.[17,18] Such coiled-coil structures have been formed at physiological pH with high thermostability,[19,20] whereas other coiled-coils have incorporated phenylalanine and tryptophan zipper motifs.[21,22] Ing et al.[23] combined these concepts to form fibrils and hydrogels from designed α-helical coiled-coil peptides incorporating aromatic phenylalanine residues in order to confer electron transport properties on the resulting assembled structures. Their findings, in combination with others,[3] suggest that the dynamic interactions of aromatic amino acid side chains in peptide-based structures can increase electrical conductivity.

Herein, we present the formation, characterization, and conductivity of newly designed, tailored, fibril-forming peptide

Received: August 30, 2018
Accepted: January 3, 2019
Published: January 22, 2019

DOI: 10.1021/acsomega.8b02231
ACS Omega 2019, 4, 1748−1756

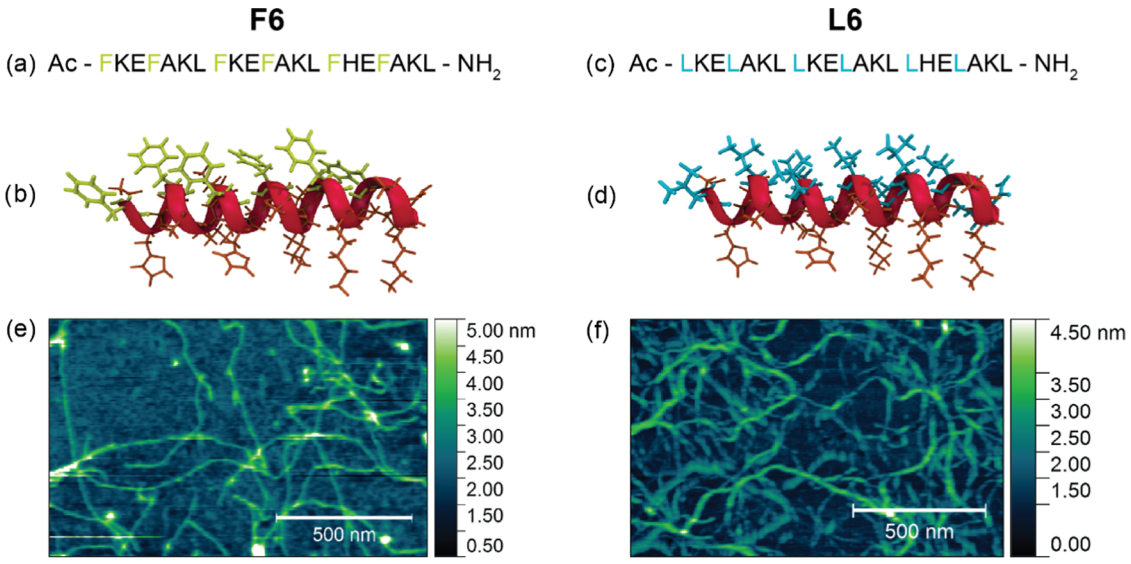

Figure 1. Amino acid sequence (a, c), secondary structure representation showing side chains (b, d), and atomic force microscopy (AFM) topography images for F6 (e) and L6 (f). Scale bars on AFM images: 500 nm (x) and 4.5 nm (z).

hydrogels in a reproducible manner. Thus, we have expanded the knowledge basis for designing electrically conductive biological nanowires, while also suggesting insightful methodology for further investigations.

RESULTS AND DISCUSSION

Fibril-Based Hydrogels. Two peptides (labeled F6 and L6) were designed for this study that were tailored to form into self-assembled nanofibrils under physiological conditions based on the coiled-coil sequence of AFD36.[20] F6 was the sequence designed to be "conductive" through incorporation of the aromatic amino acid phenylalanine (F) (Figure 1a,b) into the hydrophobic core to provide a conductive pathway.

By contrast, L6 contained no aromatic groups and was intended as the fibril-forming, but nonconducting, reference (Figure 1c,d). As with AFD36, these gels did successfully form from fibrils—seen in diluted form in Figure 1e,f. Several polymorphisms were noted for F6, including rodlike needles (Figure S1e), a twisted and tangled morphology (Figure S1d), and a twisted rodlike combination (Figure S1f). For L6, only a single morphology was observed, which was the twisted and tangled form. It should be noted that, particularly in the case of F6, fibrils were rarely observed in isolation and required specific preparation for imaging (see methods). As with the parent sequence, L6 and F6 formed a gel at around physiological pH via titration in sodium bicarbonate, allowing handling time for the pregelled solution to be placed onto interdigitated array (IDA) electrodes before fully gelling in situ, ready for assessment of conductivity.

Electrical Measurements. Some methods for potentially investigating individual fibrils may be similar to those used for pili or other nanowires,[1] such as through the use of nanofabricated electrodes,[24] conducting AFM,[25,26] or multiple-probe AFM,[27,28] if peptide fibrils prove mechanically adaptable to these procedures. We have chosen to use IDA electrodes, commonly used for measuring conductivity in nanowire films.[29−31] One of the reported reasons for using IDAs for this type of measurement is that they comprise long interdigitated electrodes separated by a small gap, thereby enhancing sensitivity and detection limits.[30] However, there are some drawbacks to this measurement system. Contact resistance cannot be considered without carrying out measurements on IDAs of several different gap sizes, increasing the time and cost of experiments. Even considering electrode-contact resistance, there is no experimental way to account for fibril-to-fibril contact (contributing also to sample capacitance) on a bulk material. In a recent paper by Ing et al.,[23] lower concentrations of peptide (relating to lower assembly and branching) resulted in increasing conductance, likely due to decreasing fibril−fibril contact resistance.

However, by careful consideration of the material properties (such as thickness dependence) and measurement conditions (such as voltage range and stable current), reproducible measurements can be made using little material, even for small electronic conductivities. Thus, an avenue for exploration for bulk materials of this nature is to determine the missing conditions to satisfy all parameters of this system, fitting the model to account for contact resistance, sample capacitance, mixed mobility carriers, and the energetics of the material.

The current−voltage (IV) curves obtained for both F6 and L6 displayed a non-Ohmic "S" shape (Figure 2), often observed for organic semiconductors such as DNA[32] and conducting polymers.[25]

At every voltage point, F6 showed a higher current response (Figure 2, upper graph) compared to L6 (Figure 2, lower graph), and the S-shape of the F6 curve was less pronounced than the L6 curve, consistent with an increase in conductivity.[24,35−37] The shape of the IV curves is indicative of space charge limited current.[33,34]

The thickness of *G. sulfurreducens* biofilms in conductivity measurements on IDAs has been reported to be 40−60[29] and 80 ± 9 μm (N = 3);[38] however, biofilms are a composite of materials and not directly comparable. Our films are thin (maximum 7.5 and 29.6 μm for F6 and L6, respectively) and difficult to compare between L6 and F6. Hence, films of various thicknesses were tested (Figure S1 for F6 and Figure S2 for L6); the consistency of these data showed that the IV response was independent of film thickness. As these materials are chemically similar, it is assumed that the electrode-contact resistance is conserved.

DOI: 10.1021/acsomega.8b02231
ACS Omega 2019, 4, 1748−1756

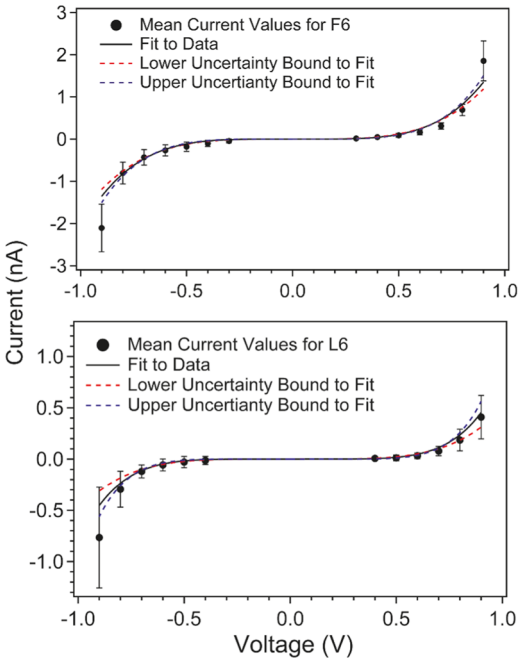

Figure 2. Current−voltage (*IV*) data for peptides F6 (top) and L6 (bottom), which have been determined from multiple samples (see Figures S2 and S3). Both peptide films demonstrate nonlinear behavior of the voltage range. Each data set has been fitted to a power law ($I = G_0V^{\alpha}$), where for F6, $\alpha_{F6} = 4.2 \pm 0.4$ (2SE) $G_{0F6} = 2.1 \pm 0.3 \times 10^{-9}$ S/V$^{3.2}$ (2SE), and for L6, $\alpha_{L6} = 5.5 \pm 1.1$ (2SE) $G_{0L6} = 8.1 \pm 0.3 \times 10^{-9}$ S/V$^{4.5}$ (2SE). The magnitude of the powers indicates that the films are behaving in a trap-limited current regime.[33,34]

As a result, a master *IV* curve for each peptide was constructed by averaging current values at a specific voltage and determining the uncertainty to 2 times the standard error (2SE) (see Figure 2). These master curves were then fitted to a power equation (eq 1)

$$I = G_0V^{\alpha} \tag{1}$$

and values for the pre-exponential and powers determined to ±2 SE.

To compare the conductivity of F6 peptide films to the control L6 films, we note two things:

(1) The *IV* curves are nonlinear; hence, a standard approach of linear fitting in the Ohmic regime is not possible.
(2) The *IV* curves showed thickness-independent behavior, excusing extensive geometric considerations.

To tackle the first point, we determined conductance ($G(V)$) values at each specific voltage for the master curves by noting that

$$I(V) = G(V)V \tag{2}$$

To tackle the second point, we used the conductance values to determine a voltage-dependent conductivity (eq 3), utilizing the fact we are in a "thick film" regime[29−31]

$$\sigma(V) = G(V)/S \tag{3}$$

where S is the form factor (determined to be 5.86 cm for our IDAs). Once we determined these individual conductivity values at each measurement point (Table S1), a ratio of the conductivities of the peptides was taken, that is, eq 4

$$\sigma(V)_{F6}/\sigma(V)_{L6} \tag{4}$$

This produced a graph from which an overall weighted mean ratio was determined with associated uncertainty via standard error propagation (Figure 3).

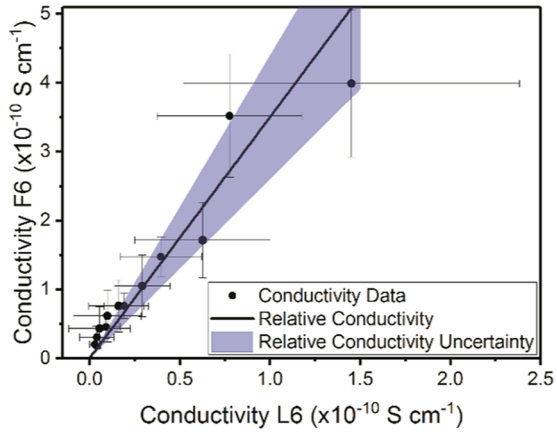

Figure 3. Ratio of the voltage-dependent conductivities between F6 and L6 peptide films. The data indicates a consistent ratio as a function of voltage across the entire voltage range, though noting that the uncertainty increases for smaller values of voltage. The solid line indicates the weighted mean value, and the shaded area indicates the uncertainty around the mean. Corresponding values are 3.5 ± 0.9 (2SE), indicating that F6 is indeed more conductive than L6.

The data shows that F6 is 3.5 ± 0.9 times more conductive than L6. However, both peptide films are still in the insulating regime, with the calculated conductivities falling in the range 10^{-9} S/m, and the magnitude of power fitting (Figure 2) indicates that the films are behaving in a space charge (trap) limited current regime.[33,34] The current is dominated by charge carriers injected from the contacts and hence the higher current at higher voltages. At low potentials, contact effects dominate the data. This type of transport has been observed using conducting probe AFM measurements on Geobacter pili WT and Y27A,[39] also displaying S-shaped *I*/*V* curves (Figure 2). The current generated from the F6 film, compared with the isolated pili from the aforementioned study, was higher than Y27A and similar to WT. Since there was no metal or redox cofactor in our peptides, this points to effective aromatic contribution to the peptide conductivity when compared to WT. However, due to lack of *I*/*V* data on isolated peptide fibrils, it was not possible to calculate carrier mobility transport and, more importantly, the effective electron carrier concentration to compare with other nanowire systems and organic semiconductors.

Our measured conductivity is slightly lower than a comparable study using films of modified Curli protein fibers (0.3−2 nS/cm).[40] The closest analogue to our work, the study by Ing et al.[23] on biomimetic α-helical peptide gels, does not report the conductivity or measured current of gel measurements. The calculated conductance values were higher (0.1−0.2 mS), suggesting increased conductivity. Fiber films prepared on IDAs showed very high conductivity, in the range of 1 S/cm, with a strong inverse correlation on fiber concentration. Our observed conductivity (nS/m range) is also significantly lower than the microbial nanowires that inspired this work (Table S1); however, to the best of our knowledge, no conductivity measurements that are directly comparable currently exist.

DOI: 10.1021/acsomega.8b02231
ACS Omega 2019, 4, 1748−1756

We have reported a relatively simple method for measuring the conductivity of high-resistance organic films; importantly, these measurements are reproducible and amenable to alteration of environment for interrogating the mechanism of conduction. Experiments that also facilitate changing of the temperature[23] and hydration status of the gels will yield further fundamental information about the electron transport mechanism in similar systems.

Conformation. Here, our de novo designed peptides incorporating a phenylalanine core showed enhanced conductivity compared to the control peptide of a leucine-based coiled-coil. We suggest that the enhanced conductivity is due to both self-assembly and the presence of phenylalanine. One of the reasons for choosing phenylalanine in the design of F6 was to enable aromatic molecular orbital overlap, potentially leading to electron delocalization and allowing band-gap behavior. Some literature cites this as the mechanism of the conductivity of *G. sulfurreducens*.[23,29,41] To investigate the electronic state of phenylalanine in these peptides, fluorescence spectroscopy was undertaken as the Stokes shift of phenylalanine emission peaks has been attributed to $\pi-\pi$ stacking in the literature.[42−44] As seen in Figure 4, such a Stokes shift is observed in F6 at 304 nm, suggesting interaction between the phenylalanine groups of the peptide monomers.

When excited at 265 nm, F6 showed the expected emission at around 280 nm due to phenylalanine, regardless of buffer. As such, the peak intensities of all samples were normalized to the phenylalanine peak at 280 nm for easy comparison. The peak at 304 nm also had a shoulder around 315 nm, followed by a long tail-off as the emission slowly reapproached zero. The additional peak, shoulder, and tail-off is of higher intensity in the sample of F6 in water (acidic; Figure 3a, dotted black line) relative to the phenylalanine peak at 280 nm.

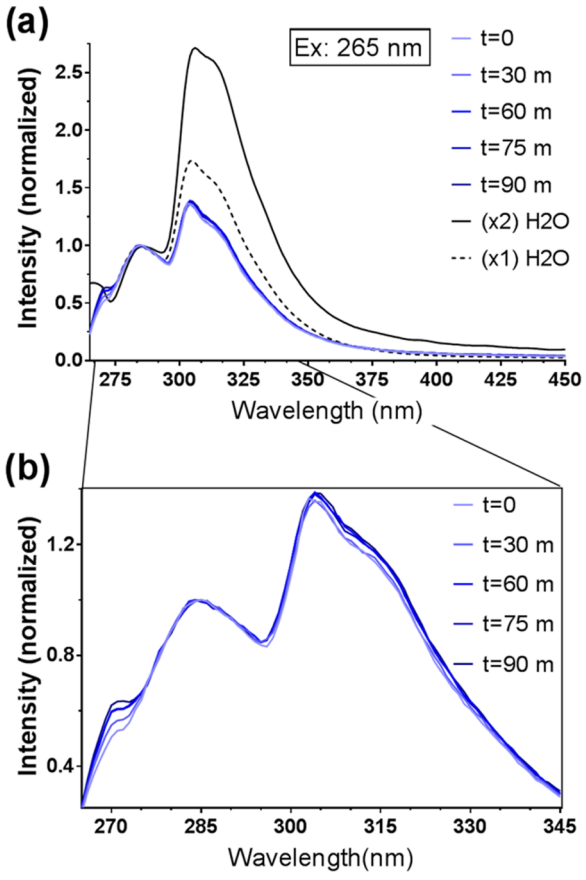

Figure 4. Fluorescence emission spectra with an excitation wavelength of 265 nm of F6 peptide in (black lines) water and (blue lines) titrated over time with sodium bicarbonate, where (b) is a portion of (a) omitting water and zoomed in on the region of interest for clarity.

To compare the effect of pH changes on the same sample and ensure no other inconsistencies in concentration or sample preparation, a time series was undertaken during gelation following addition of sodium bicarbonate to F6. The initial F6 concentration was 10 mM (Figure 4a, solid black line) before addition of sodium bicarbonate and showed the largest relative intensity of fluorescence emission at 315 nm of all measured samples. During pH change, the biggest spectral change can be seen at the peak near 270 nm (Figure 4b), which increased in intensity as the sample approached pH 7.4 over time. More subtle changes were observed in peaks at higher wavelengths relative to the phenylalanine peak at 280 nm. The peak at 304 nm and the following shoulder near 315 nm increased in intensity after 60 min, suggesting increasing aromatic interactions due to gelation.

By contrast, L6 samples did not show significant emission spectra, with a small emission at around 310 nm, potentially due to histidine residues (Figure S4). The negative controls of the empty cuvette and water alone did not show fluorescence emission (Figure S4).

The substantial increase in intensity of the emissions above 280 nm in the nongelled samples may reflect the presence of oligomers in solution (Figure 4a). This is supported by secondary structure investigations as α helices were detected by circular dichroism (CD) spectroscopy even at low concentrations and under acidic conditions (Figure 5).

The canonical α helical shape[45,46] was observed by CD for all concentrations and buffers of L6, with the double minimum around 208 and 222 nm and a positive peak at ∼195 nm (Figure 5a,c). Although changing the pH at high concentration (1 mM) did not result in a significant change in the shape of the CD spectra, dropping the concentration of L6 in water did reduce the intensity of the peaks, indicative of a change in conformation toward random coil.[47] The α helical shape was also observed by CD for F6; however, it appeared to be distorted. The double minimum at around 208 and 222 nm was less defined and red-shifted (Figure 5b,d). Similar features were observed for gel films measured in a dry state (Figure S5).

As α helices are not stable as monomers, it is reasonable to suggest that assembly is occurring, and the hydrophobic phenylalanine groups are associating in the aggregated structure. As seen in Figure 5, the L6 peptide formed α helices as predicted, suggesting a coiled-coil structure as described in similar systems.[19,20] However, the same type of spectra was not observed for F6, even accounting for some distortion due to aromatics in the CD spectrum.[45,48] The presence of antiparallel β-sheets, type II β-turns, or aggregates in solution may account for the red-shifting and reduced intensity of the peak at 208 nm.[45,46] It is interesting to note that significant effects due to change of pH were not observed as seen in similar peptide sequences;[19,20] in both L6 and F6, the minima at around 208 and 222 nm are not significantly higher after adjusting the pH close to the gelation set point of 7.4 (Figure 5c,d). In the case of L6, the α helical shape was close to its final intensity even in water (Figure 5a, red line); however, F6 had a strong increase in intensity when placed into buffer for pH adjustment (Figure 5a, red line, compared to

DOI: 10.1021/acsomega.8b02231
ACS Omega 2019, 4, 1748−1756

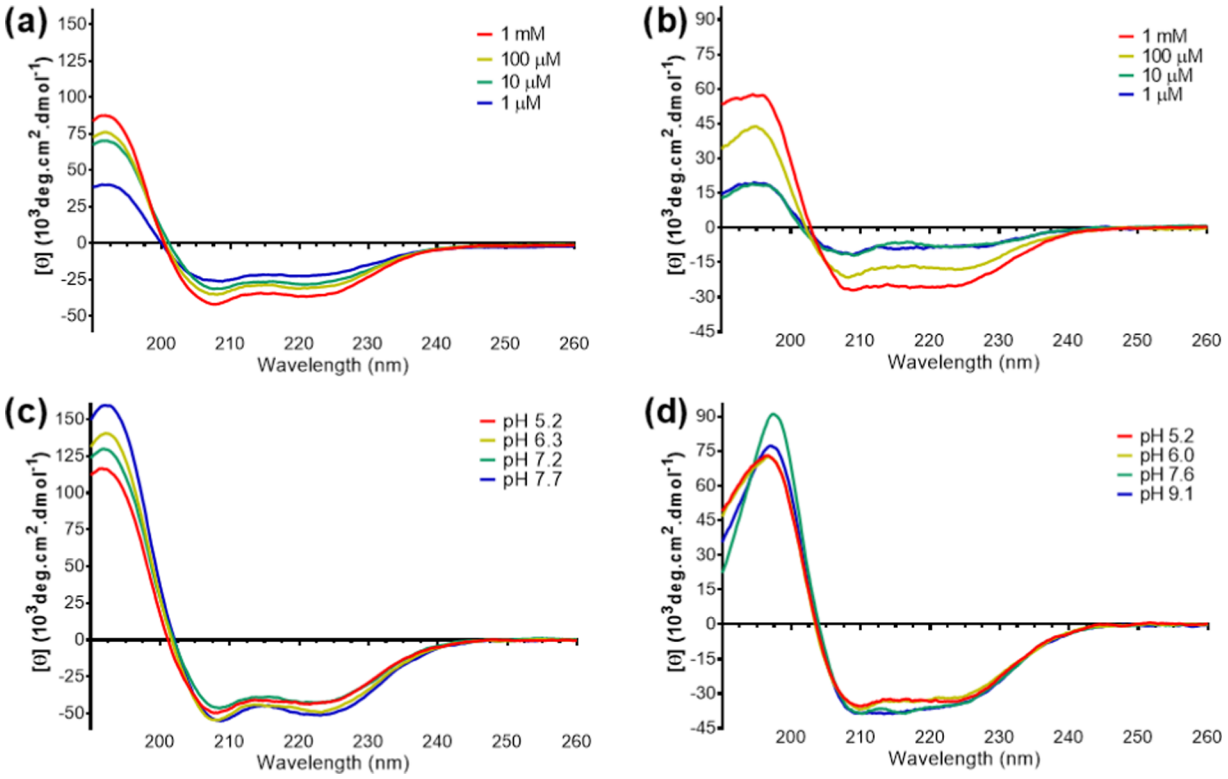

Figure 5. CD spectroscopies of (a, c) L6 and (b, d) F6 peptides. (a, b) Dilution series of peptides in water, showing a change toward random coil configuration at lower concentrations (per legend) and (c, d) CD spectra of 1 mM peptides in 10 mM 2-(*N*-morpholino)ethanesulfonic acid buffer at varying pH (per legend), adjusted using NaOH.

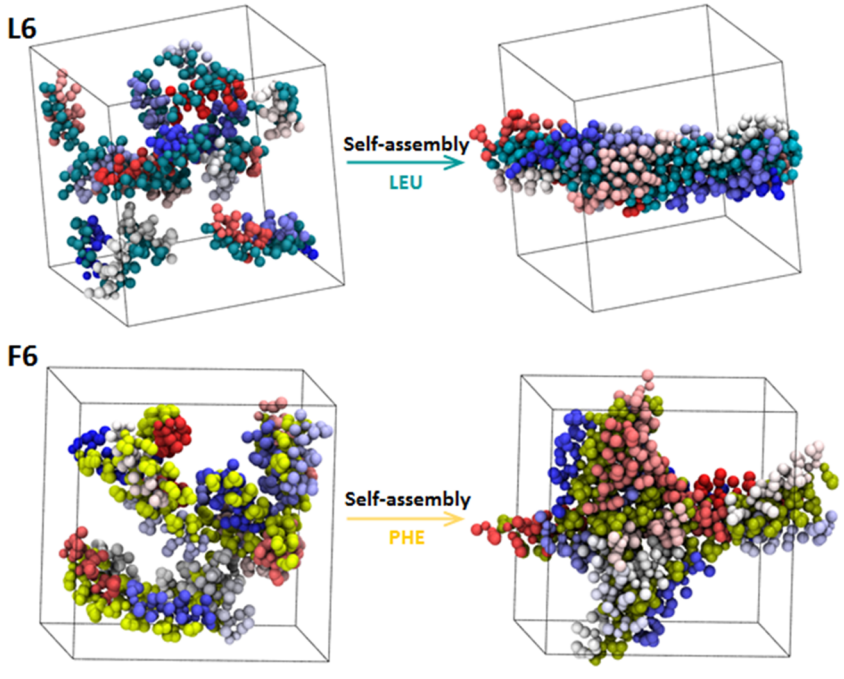

Figure 6. Self-assembly of L6 (above) and F6 (below) into nanofibrils as obtained from MD simulations using the coarse-grained MARTINI model for the peptides. On the left are snapshots of L6 and F6 peptides randomly distributed inside simulation boxes with leucine and phenylalanine shown in green and yellow, respectively, and different peptide chains presented in different colors. On the right, after 10 μs simulation, L6 has assembled into a nanofibril with moment of inertia (MOI) along the principal axes of the largest cluster of 7.74, whereas F6 has assembled into a higher dimension nanofibril with MOI of 2.23.

Figure 5d, red line). Either F6 does not form assembled structures without the presence of salt/buffer or it has formed small, nonchiral oligomers in solution that do not absorb in the CD spectra. Given the strong fluorescence peaks, the former would appear to be more likely. F6 gels readily at the

DOI: 10.1021/acsomega.8b02231
ACS Omega 2019, 4, 1748−1756

appropriate pH, suggesting these early oligomers are in equilibrium rather than overcoming a nucleation barrier.

Simulations. For 21-mer peptides such as F6 and L6, the formed helical structures have bent rather than extended helical conformation, based on molecular simulation (Figure S6). Full-atomic molecular dynamics (MD) simulations show that F6 possesses a stable α-helix secondary structure, like its parent sequence AFD36.[19,20] However, the peptide ends may be more flexible, showing allowed conformations in the polyproline or extended β-sheet regions for the first and last heptads. Overall, F6 was stabilized into a helix-turn-helix conformation, as verified by the highly populated cluster. It is possible that the favored interactions between the aromatic amino acids of side chains exceed the interaction of backbone hydrogen bonds, which results in the bending of the extended helix. This finding is similar to the folding simulation of long proteins reported by Lazim et al.[49] and Duan et al.[50] To be clear, L6 was seen by contrast to adopt a stable α-helix conformation, in agreement with the CD data (Figure 5). As F6 displays a less stable helix, it is less likely to form perfect coiled-coil structures—as evidenced by the experimental results, seen in the form of multiple fibril polymorphisms and imperfect CD curves.

Coarse-grained (CG) assembly simulations were carried out up to 40 μs to investigate the likely structure of assembled fibrils, shown in Figure 6. F6 tended to form an aggregated structure with dimension >1. The aggregation propensity score, calculated as the ratio of the solvent-accessible surface area (SASA) of the peptide molecules in the initial minimized box to the SASA of the final configuration of the simulation of F6, is smaller than that for L6 (from both full-atomic and coarse-grained Martini approaches). The moment of inertia (MOI) of F6 is similar in all three dimensions, thus confirming the observation that the F6 aggregated structure has dimension >1.

As expected, L6 was observed to form one-dimensional (1D) fibril structures based on the coiled-coil motif. Interestingly, F6 formed fibrillar-like structures but did not continue in the form of 1D assembly. Instead, the bent-helix lent itself to branching, resulting in a meshlike structure. However, as highlighted in blue and yellow, which represent leucine and phenylalanine, respectively, the hydrophobic residues remained as expected within the core of the assembled structures (Figure 6, right). It is possible that the interaction between phenylalanine residues triggered both intramolecular (end-bending) and intermolecular interactions. Despite these different fibrillar-like structures, the aggregation did bring the benzene rings of phenylalanine into close proximity as can be seen from the radial distribution function (RDF; Figure 7).

Confirming the fluorescence data in Figure 4, the RDF calculation in Figure 7 shows interaction of benzene rings in F6 after self-assembly. Importantly, a portion of the phenylalanine residues are within 3−5 Å of another phenylalanine, suggesting conditions conducive to electron transfer.[1,51] These data do not reflect the conformation of the benzene rings and therefore cannot, alone, confirm $\pi-\pi$ stacking.

As highlighted, the low conductivity achieved is likely due to poor fibril−fibril contact and broken electron transfer pathways from branching and multiple polymorphisms. From these simulations, we conclude that refining the design through smarter placement of the bulky phenylalanine residues would enhance conductivity. By reducing bending of the helix residue by moving the phenylalanine away from the ends of the sequence, two-dimensional assembly and conductivity would be enhanced.

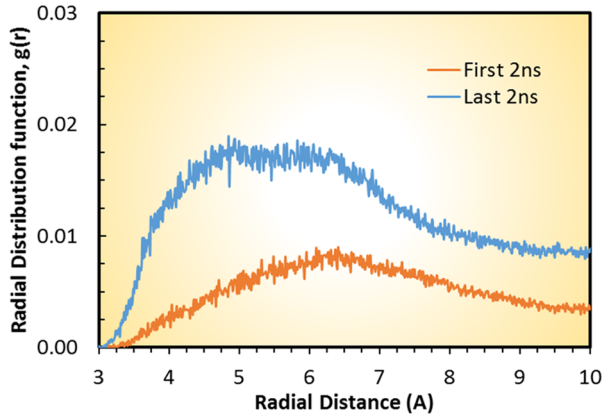

Figure 7. Radial distribution of interaromatic rings shows possibility of intermolecular aromatic ring-stacking interactions at high concentration of F6 peptide. Data were extracted from full-atomic MD simulation of 28xF6 peptides (starting from random distribution in a periodic simulation box) at 500 ns.

CONCLUSIONS

The most important features of this work have been the de novo design of peptides for self-assembly and enhanced conductivity and the development of reliable methods for the electronic investigation of biomolecules. Using steady-state conditions for films of varying thicknesses drop cast onto IDAs, current−voltage plots can be formulated through the equations given herein for high-resistance organic materials.

We can say that de novo designed peptides incorporating a phenylalanine core show enhanced conductivity compared to the control peptide of a leucine-based coiled-coil. Through electronic, spectroscopic, and simulation analyses, we suggest that the enhanced conductivity is due to both self-assembly into fibrillary form and the presence of phenylalanine.

This work offers additional phenomenological evidence to suggest that amino acids are capable of transporting electrons across micron-scale distances without the aid of redox centers or metal components. Taken together, the results provide support for electron delocalization as playing a role in *G. sulfurreducens* pili, although there is still some way to go to optimize phenylalanine as a sole mobility carrier in assembled peptide systems. Improved structures could be formed by replacement/addition of phenylalanine by another electronically active moiety, such as tryptophan, or through stabilization of the C-terminus region to improve 1D self-assembly. Adornment of the fibrils or gels using a hopping stepping stone may also assist in conductivity by offering conduits for electron hopping between fibrils.

EXPERIMENTAL SECTION

Peptide Preparation. Peptides L6 (Ac-LHELAKL LHELAKL LKELAKL-$CONH_2$, MW 2465.04 g/mol) and F6 (Ac-FHEFAKL FHEFAKL FKEFAKL-$CONH_2$, MW 2669.14 g/mol) were synthesized and purified by GenScript and Mimotopes (Australia) using FMOC chemistry. The final purity was >95% as measured by high-performance liquid chromatography. The peptide content of the solid was determined by high-sensitivity amino acid analysis for precise

DOI: 10.1021/acsomega.8b02231
ACS Omega 2019, 4, 1748−1756

concentration calculations (Australian Proteome Analysis Facility, Sydney).

Peptide stocks were prepared from lyophilized powder in water (Ultrapure MilliQ, 18.2 MΩ) at a concentration of 10 mM (36.4 and 37.7 mg/mL for F6 and L6, respectively) and further diluted in desired buffer as required.

Conductivity. Electrical measurements were carried out on films prepared on interdigitated array (IDA) microelectrodes (ED-IDA6-Au, Micrux Technologies, Spain). The IDAs had a channel length of 1500 μm, width of 5 μm, electrode gap of 5 μm, and the number of electrode fingers was 30.

Arrays were electrochemically cleaned in 0.1 M H_2SO_4 as per the manufacturer's instructions and tested as a negative control; then, the sample was drop cast and dried in air prior to measurement. For thicker films, 2 μL of sample was drop cast, whereas for thinner films (under 1 μm thickness), the excess amount of sample was removed almost immediately after the sample was drop cast by gently scraping a clean glass slide across the IDA. Arrays were checked for damage by optical microscopy. After electrical measurement, film heights were measured using a Dektak 150 stylus profiler (Bruker, Germany).

Two-point probe current−voltage (*IV*) data was constructed utilizing previously published methods[29] in which a set voltage was applied across the film and the current recorded up to 100 s to minimize the ionic contribution over time. The final equilibrium result was taken as the electronic current value for the film. Discrete voltage values were selected from −0.9 to 0.9 V in 0.1 V steps to yield the final *IV* curves. Data was obtained by utilizing a probe station connected to an Agilent B1500A Semiconductor Parameter Analyser (Keysight Technologies). Our voltage range selection was chosen to be below 1.2 V so as to avoid electrochemical splitting of water.

We were unable to obtain reliable current values for our films from −0.3 to 0.3 V due to insufficient equipment sensitivity; hence, current measurements in this range were not recorded.

Circular Dichroism. CD spectra were recorded using a JASCO J-815 CD spectrophotometer at 20 °C in 0.1−10 mm quartz cuvettes. Spectra were recorded from 190 to 260 nm with a step size of 0.1 nm, bandwidth of 1 nm, integration time of 4 s, and averaged over 10 scans. Raw ellipticities were converted to mean residue ellipticities as described previously.[20]

Molecular Dynamics Simulations. All-atom molecular dynamics simulation was conducted to get more information on the secondary structures of the designed peptides. The initial structures of F6 and L6 were built in (right-hand) α-helix conformation of 21 amino acids by PyMOL and were capped on the N-terminus with an acetyl group and on the C-terminus with a primary amide ($CONH_2$). Peptides were then immersed in the center of cubic periodic (in all directions) TIP3P water boxes with the minimum solute-box boundary distance being set to 1.5 nm to ensure the absence of periodic image interactions. Counterions were added to produce a neutral simulation system. The salt concentration (NaCl) was set at 50 mM. MD simulations were driven by the GROMACS 5.1 software package with CHARMM36 force field for the peptides. The LINCS algorithm was applied to constrain all bond lengths between heavy atoms and hydrogen atoms.[52] The Verlet leapfrog algorithm was used to propagate the dynamics of the system at a time step of 2 fs. The long-range electrostatic interaction was treated with the particle-mesh-Ewald method, and the van der Waals interactions were calculated with a cutoff at 1.2 nm. Each system initially underwent 10 000 steps of steepest descent to remove the local strain in the peptide (due to generation of hydrogen positions) and to remove bad van der Waals contacts, followed by 50 000 steps with position restrains on the heavy atoms, the backbone atoms, and the C_α atoms. The simulation was continued with the NPT ensemble at temperature of 298 K and 1 bar pressure employing the Nosé−Hoover thermostat and the Parrinello−Rahman barostat, respectively. Initial velocities were generated according to the Maxwell distribution. The coordinates and velocities were monitored every 2 ps, and the energies were recorded every 5 ps. Backbone dihedral angles ψ against φ of amino acid residues in L6 and F6 were determined by the GROMACS command g_rama. The pair distribution function $g(r)$ between the aromatic rings of PHE was determined using VMD for the last 2 ns of the production run. The first 200 ns runs of each trajectory were omitted to reduce the bias of the respective starting model. All visualizations were produced by VMD with the Tk Console extension tool.

To get more insight into the fibril assembly process, MD simulations with the coarse-grained (CG) MARTINI force field were also conducted for F6 and L6. The (right-hand) α-helix conformation was used as the secondary structure of both peptides. CG Martini topologies of the peptides were built using the martinize.py script. This force field uses a 4:1 atom/CG-bead mapping to represent peptide backbone and side chains and a 3:1 atom/CG-bead mapping for the aromatic ring of PHE. The CG MARTINI model does provide insight into the driving force for the aggregation and consequently the self-assembly of peptides, even though the priori secondary structures are fixed during the simulation and the polarity, shape, and nonbonded interaction potential of the amino acids only included implicitly. Eighteen peptides were initially placed randomly in a cubic simulation box of $8 \times 8 \times 8$ nm^3 and then solvated in Martini water.[23,53] The coarse-grained MD simulations were run in the NPT ensemble. The Berendsen method was used to maintain the pressure and temperature at 1 bar and 303 K, respectively. The systems were simulated for 40 μs in effective simulation time. To get more insight into the structure (one-dimensionality) of self-assembled fibers after the production run, we calculated the moments of inertia (MOIs) along the principal axes of the system of the largest cluster of peptides. In detail, the cluster was centered and aligned according to its principal axes. The moments of inertia of the cluster in the final snapshot are calculated by the GROMACS command g_gyrate. The aspect ratios (I_z/I_x) and relative magnitudes of I_x, I_y, and I_z give some insight into the differences in self-assembled structures. Aggregates with $I_x \ll I_y \approx I_z$ are mainly 1D.

Atomic Force Microscopy. AFM micrographs were collected using an Asylum MFP3D SPM (Oxford Instruments) using Etalon HA NC probes (nom k = 3.5 N/m, nom f = 140 kHz) in the tapping mode under ambient conditions. Peptide samples were freshly prepared to 10 mM in water (Ultrapure MilliQ, 18.2 MΩ) and then diluted to a final concentration of 1 mM in 5.04 or 5.26 mM (for F6 or L6, respectively) $NaHCO_3$. Then, 20−50 μL of sample was spotted onto OTS-coated silicon wafer[54] and incubated for 2 h in a humid environment. Excess liquid was removed by wicking; then, samples were rinsed in 10 mM $NaHCO_3$ (adjusted to pH 7.4 with HCl) and allowed to dry in air before imaging. Fibrils were easily found in the optically clear areas within ∼100−200

DOI: 10.1021/acsomega.8b02231
ACS Omega 2019, 4, 1748−1756

μm of micron-scale salt crystals. Image analysis was undertaken using freeware Gwyddion (http://gwyddion.net) v2.41.

Fluorescence Spectroscopy. Fluorescence spectroscopy measurements were carried out at room temperature on a Jobin Yvon Fluoromax 4 (Horiba, Japan) fluorescence spectrophotometer with a small-volume cuvette (pathlength 0.1 cm) with excitation wavelength of 265 nm, emission wavelength in the range of 275−500 nm, and a scan speed of ∼250 nm/min. Emission data was normalized against the fluorescence peak of phenylalanine (280 nm).

■ ASSOCIATED CONTENT

Supporting Information

The Supporting Information is available free of charge on the ACS Publications website at DOI: 10.1021/acsomega.8b02231.

AFM micrographs of additional F6 morphologies, derivation of the units for G_0, *IV* curves for F6 and L6, fluorescence emission spectra blanks/controls, and secondary structure propensity from modeling of L6 and F6 (PDF)

■ AUTHOR INFORMATION

Corresponding Authors

*E-mail: Rhiannon.creasey@gmail.com (R.C.G.C.).
*E-mail: b.laycock@uq.edu.au (B.L.).

ORCID

Rhiannon C. G. Creasey: 0000-0003-4780-4623
Tuan A. H. Nguyen: 0000-0002-3024-2081
Bernardino Virdis: 0000-0001-8036-8937
Stefano Freguia: 0000-0002-2294-9036

Present Address

[‖]Sustainable Minerals Institute, The University of Queensland, St Lucia, QLD 4072, Australia (T.A.H.N.).

Author Contributions

The manuscript was written through contributions of all authors. All authors have given approval to the final version of the manuscript.

Notes

The authors declare no competing financial interest.

■ ACKNOWLEDGMENTS

This research was facilitated using infrastructure provided by the Australian Government through the National Collaborative Research Infrastructure Strategy (NCRIS) by access to the Australian Proteome Analysis Facility and the Queensland node of the Australian National Fabrication Facility (ANFF). Financial support was provided by the Australian Research Council (Grant ID DP150100268 and DP140103653). A.S. is supported by the Australian Government Research Training Program (RTP) Scholarship. A.B.M. is a Sêr Cymru II fellow, and results incorporated in this work have received funding from the European Union's Horizon 2020 research and innovation program under the Marie Skłodowska-Curie grant agreement No. 663830.

■ REFERENCES

(1) Creasey, R. C. G.; Mostert, A. B.; Nguyen, T. A. H.; Virdis, B.; Freguia, S.; Laycock, B. Microbial nanowires − Electron transport and the role of synthetic analogues. *Acta Biomater.* **2018**, *69*, 1−30.
(2) Lovley, D. R. Electrically conductive pili: Biological function and potential applications in electronics. *Curr. Opin. Electrochem.* **2017**, *4*, 190−198.
(3) Ing, N. L.; El-Naggar, M. Y.; Hochbaum, A. I. Going the Distance: Long-Range Conductivity in Protein and Peptide Bioelectronic Materials. *J. Phys. Chem. B* **2018**, 10403−10423.
(4) Malvankar, N.; Lovley, D. Microbial Nanowires: A New Paradigm for Biological Electron Transfer and Bioelectronics. *ChemSusChem* **2012**, *5*, 1039−1046.
(5) Lovley, D. R. Electromicrobiology. *Annu. Rev. Microbiol.* **2012**, *66*, 391−409.
(6) Malvankar, N. S.; Lovley, D. R. Microbial nanowires for bioenergy applications. *Curr. Opin. Biotechnol.* **2014**, *27*, 88−95.
(7) Zacharoff, L. A.; El-Naggar, M. Y. Redox conduction in biofilms: From respiration to living electronics. *Curr. Opin. Electrochem.* **2017**, 182−189.
(8) Nealson, K. H. Geomicrobiology: Sediment reactions defy dogma. *Nature* **2010**, *463*, 1033−1034.
(9) Bjerg, J. T.; Boschker, H. T.; Larsen, S.; Berry, D.; Schmid, M.; Millo, D.; Tataru, P.; Meysman, F. J.; Wagner, M.; Nielsen, L. P.; Schramm, A. Long-distance electron transport in individual, living cable bacteria. *Proc. Natl. Acad. Sci. U.S.A.* **2018**, *115*, 5786−5791.
(10) Shi, L.; Dong, H.; Reguera, G.; Beyenal, H.; Lu, A.; Liu, J.; Yu, H.-Q.; Fredrickson, J. K. Extracellular electron transfer mechanisms between microorganisms and minerals. *Nat. Rev. Microbiol.* **2016**, *14*, 651−662.
(11) Berggren, M.; Richter-Dahlfors, A. Organic bioelectronics. *Adv. Mater.* **2007**, *19*, 3201−3213.
(12) Rivnay, J.; Owens, R. M.; Malliaras, G. G. The Rise of Organic Bioelectronics. *Chem. Mater.* **2014**, *26*, 679−685.
(13) Tan, Y.; Adhikari, R. Y.; Malvankar, N. S.; Ward, J. E.; Woodard, T. L.; Nevin, K. P.; Lovley, D. R. Expressing the Geobacter Metallireducens PilA in *Geobacter sulfurreducens* Yields Pili with Exceptional Conductivity. *mBio* **2017**, *8*, No. e02203.
(14) Zhang, S. Fabrication of novel biomaterials through molecular self-assembly. *Nat. Biotechnol.* **2003**, *21*, 1171−1178.
(15) Guterman, T.; Kornreich, M.; Stern, A.; Adler-Abramovich, L.; Porath, D.; Beck, R.; Shimon, L. J. W.; Gazit, E. Formation of bacterial pilus-like nanofibres by designed minimalistic self-assembling peptides. *Nat. Commun.* **2016**, *7*, No. 13482.
(16) Reardon, P. N.; Mueller, K. T. Structure of the Type IVa Major Pilin from the Electrically Conductive Bacterial Nanowires of *Geobacter sulfurreducens*. *J. Biol. Chem.* **2013**, *288*, 29260−29266.
(17) Ryadnov, M. G.; Woolfson, D. N. Engineering the morphology of a self-assembling protein fibre. *Nat. Mater.* **2003**, *2*, 329−332.
(18) Woolfson, D. N.; Mahmoud, Z. N. More than just bare scaffolds: towards multi-component and decorated fibrous biomaterials. *Chem. Soc. Rev.* **2010**, *39*, 3464−3479.
(19) Fletcher, N. L.; Lockett, C. V.; Dexter, A. F. A pH-responsive coiled-coil peptide hydrogel. *Soft Matter* **2011**, *7*, 10210−10218.
(20) Dexter, A. F.; Fletcher, N. L.; Creasey, R. G.; Filardo, F.; Boehm, M. W.; Jack, K. S. Fabrication and characterization of hydrogels formed from designer coiled-coil fibril-forming peptides. *RSC Adv.* **2017**, *7*, 27260−27271.
(21) Liu, J.; Zheng, Q.; Deng, Y. Q.; Kallenbach, N. R.; Lu, M. Conformational transition between four and five-stranded phenylalanine zippers determined by a local packing interaction. *J. Mol. Biol.* **2006**, *361*, 168−179.
(22) Liu, J.; Yong, W.; Deng, Y. Q.; Kallenbach, N. R.; Lu, M. Atomic structure of a tryptophan-zipper pentamer. *Proc. Natl. Acad. Sci. U.S.A.* **2004**, *101*, 16156−16161.
(23) Ing, N. L.; Spencer, R. K.; Luong, S. H.; Nguyen, H. D.; Hochbaum, A. I. Electronic Conductivity in Biomimetic α-Helical Peptide Nanofibers and Gels. *ACS Nano* **2018**, *12*, 2652−2661.
(24) Adhikari, R. Y.; Malvankar, N. S.; Tuominen, M. T.; Lovley, D. R. Conductivity of Individual Geobacter Pili. *RSC Adv.* **2016**, *6*, 8354.
(25) Dong, L.; Hollis, T.; Fishwick, S.; Connolly, B.; Wright, N. G.; Horrocks, B. R.; Houlton, A. Synthesis, manipulation and

DOI: 10.1021/acsomega.8b02231
ACS Omega 2019, 4, 1748−1756

conductivity of supramolecular polymer nanowires. *Chem. - Eur. J.* **2007**, *13*, 822−828.
(26) Leung, K. M.; Wanger, G.; El-Naggar, M. Y.; Gorby, Y.; Southam, G.; Lau, W. M.; Yang, J. Shewanella oneidensis MR-1 Bacterial Nanowires Exhibit p-Type, Tunable Electronic Behavior. *Nano Lett.* **2013**, *13*, 2407−2411.
(27) Higuchi, R.; Shingaya, Y.; Nakayama, T. Resistance of single polyaniline fibers and their junctions measured by double-probe atomic force microscopy. *Jpn. J. Appl. Phys.* **2016**, *55*, No. 08NB09.
(28) Higuchi, S.; Kubo, O.; Kuramochi, H.; Aono, M.; Nakayama, T. A quadruple-scanning-probe force microscope for electrical property measurements of microscopic materials. *Nanotechnology* **2011**, *22*, No. 285205.
(29) Malvankar, N. S.; Vargas, M.; Nevin, K. P.; Franks, A. E.; Leang, C.; Kim, B. C.; Inoue, K.; Mester, T.; Covalla, S. F.; Johnson, J. P.; Rotello, V. M.; Tuominen, M. T.; Lovley, D. R. Tunable metallic-like conductivity in microbial nanowire networks. *Nat. Nanotechnol.* **2011**, *6*, 573−579.
(30) Yates, M. D.; Golden, J. P.; Roy, J.; Strycharz, S. M.; Tsoi, S.; Erickson, J. S.; El-Naggar, M.; Calabrese Barton, S.; Tender, L. M. Thermally activated long range electron transport in living biofilms. *Phys. Chem. Chem. Phys.* **2015**, *17*, 32564−32570.
(31) Kankare, J.; Kupila, E. L. In-situ conductance measurement during electropolymerization. *J. Electroanal. Chem.* **1992**, *322*, 167−181.
(32) Cohen, H.; Nogues, C.; Naaman, R.; Porath, D. Direct measurement of electrical transport through single DNA molecules of complex sequence. *Proc. Natl. Acad. Sci. U.S.A.* **2005**, *102*, 11589−11593.
(33) Lampert, M. A.; Schilling, R. B. Chapter 1 Current Injection in Solids: The Regional Approximation Method. In *Semiconductors and Semimetals*; Willardson, R. K., Beer, A. C., Eds.; Elsevier, 1970; Vol. *6*, pp 1−96.
(34) Wang, D.; Shen, J. A theoretical model for carrier transport in disordered organic materials. *Synth. Met.* **2000**, *111−112*, 349−351.
(35) Lampa-Pastirk, S.; Veazey, J. P.; Walsh, K. A.; Feliciano, G. T.; Steidl, R. J.; Tessmer, S. H.; Reguera, G. Thermally activated charge transport in microbial protein nanowires. *Sci. Rep.* **2016**, *6*, No. 23517.
(36) Steidl, R.; Lampa-Pastirk, S.; Reguera, G. Mechanistic stratification in electroactive biofilms of *Geobacter sulfurreducens* mediated by pilus nanowires. *Nat. Commun.* **2016**, *7*, No. 12217.
(37) Ing, N. L.; Nusca, T. D.; Hochbaum, A. I. *Geobacter Sulfurreducens* Pili Support Ohmic Electronic Conduction in Aqueous Solution. *Phys. Chem. Chem. Phys.* **2017**, *19*, 21791.
(38) Yates, M. D.; Strycharz-Glaven, S. M.; Golden, J. P.; Roy, J.; Tsoi, S.; Erickson, J. S.; El-Naggar, M. Y.; Barton, S. C.; Tender, L. M. Measuring Conductivity of Living *Geobacter sulfurreducens* Biofilms. *Nat. Nanotechnol.* **2016**, *11*, 910.
(39) Lampa-Pastirk, S.; Veazey, J. P.; Walsh, K. A.; Feliciano, G. T.; Steidl, R. J.; Tessmer, S. H.; Reguera, G. Thermally Activated Charge Transport in Microbial Protein Nanowires. *Sci. Rep.* **2016**, *6*, No. 23517.
(40) Courchesne, N.-M. D.; DeBenedictis, E. P.; Tresback, J.; Kim, J. J.; Duraj-Thatte, A.; Zanuy, D.; Keten, S.; Joshi, N. S. Biomimetic engineering of conductive curli protein films. *Nanotechnology* **2018**, *29*, No. 454002.
(41) Ing, N. L.; Nusca, T. D.; Hochbaum, A. I. *Geobacter sulfurreducens* pili support ohmic electronic conduction in aqueous solution. *Phys. Chem. Chem. Phys.* **2017**, *19*, 21791−21799.
(42) Krysmann, M. J.; Castelletto, V.; Hamley, I. W. Fibrillisation of hydrophobically modified amyloid peptide fragments in an organic solvent. *Soft Matter* **2007**, *3*, 1401.
(43) Marshall, K. E.; Morris, K. L.; Charlton, D.; O'Reilly, N.; Lewis, L.; Walden, H.; Serpell, L. C. Hydrophobic, aromatic, and electrostatic interactions play a central role in amyloid fibril formation and stability. *Biochemistry* **2011**, *50*, 2061−2071.
(44) Creasey, R. C. G.; Shingaya, Y.; Nakayama, T. Improved electrical conductance through self-assembly of bioinspired peptides into nanoscale fibers. *Mater. Chem. Phys.* **2015**, *158*, 52−59.
(45) Fasman, G. D. *Circular Dichroism and the Conformational Analysis of Biomolecules*, 1st ed.; Springer, 1996.
(46) Greenfield, N. J. Using circular dichroism spectra to estimate protein secondary structure. *Nat. Protoc.* **2007**, *1*, 2876−2890.
(47) Chen, Y.-H.; Yang, J. T.; Chau, K. H. Determination of the helix and β form of proteins in aqueous solution by circular dichroism. *Biochemistry* **1974**, *13*, 3350−3359.
(48) Manning, M. C.; Woody, R. W. Theoretical study of the contribution of aromatic side chains to the circular dichroism of basic bovine pancreatic trypsin inhibitor. *Biochemistry* **1989**, *28*, 8609−8613.
(49) Lazim, R.; Wei, C.; Sun, T.; Zhang, D. Ab initio folding of extended α-helix: A theoretical study about the role of electrostatic polarization in the folding of helical structures. *Proteins: Struct., Funct., Bioinf.* **2013**, *81*, 1610−1620.
(50) Duan, L.; Zhu, T.; Ji, C.; Zhang, Q.; Zhang, J. Z. H. Direct folding simulation of helical proteins using an effective polarizable bond force field. *Phys. Chem. Chem. Phys.* **2017**, *19*, 15273−15284.
(51) Malvankar, N. S.; Vargas, M.; Nevin, K. P.; Tremblay, P.-L.; Evans-Lutterodt, K.; Nykypanchuk, D.; Martz, E.; Tuominen, M. T.; Lovley, D. Structural Basis for Metallic-Like Conductivity in Microbial Nanowires. *mBio* **2015**, *6*, No. e00084.
(52) Hess, B.; Bekker, H.; Berendsen, H. J. C.; Fraaije, J. G. E. M. LINCS: A linear constraint solver for molecular simulations. *J. Comput. Chem.* **1997**, *18*, 1463−1472.
(53) Sørensen, J.; Periole, X.; Skeby, K. K.; Marrink, S.-J.; Schiøtt, B. Protofibrillar Assembly Toward the Formation of Amyloid Fibrils. *J. Phys. Chem. Lett.* **2011**, *2*, 2385−2390.
(54) Nguyen, T. A. H.; Nguyen, A. V.; Hampton, M. A.; Xu, Z. P.; Huang, L.; Rudolph, V. Theoretical and experimental analysis of droplet evaporation on solid surfaces. *Chem. Eng. Sci.* **2012**, *69*, 522−529.

DOI: 10.1021/acsomega.8b02231
ACS Omega 2019, 4, 1748−1756